Available online at www.sciencedirect.com
SCIENCE DIRECT®
Journal of Magnetic Resonance 167 (2004) 49–55
JMR Journal of Magnetic Resonance
www.elsevier.com/locate/jmr

Two analytical solutions for a model of pulsed arterial spin labeling with randomized blood arrival times

J. Hrabe* and D.P. Lewis

Center for Advanced Brain Imaging, Nathan S. Kline Institute, 140 Old Orangeburg Road, Orangeburg, NY 10962, USA

Received 30 May 2003; revised 10 November 2003

Abstract

A fairly general theoretical model for pulsed arterial spin labeling perfusion methods has been available for some time but analytical solutions were derived for only a small number of arterial blood input functions. These mostly assumed a sudden and simultaneous arrival of the tagged blood into the imaged region. More general cases had to be handled numerically. We present analytical solutions for two more realistic arterial input functions. They both allow the arrival times of the molecules of tagged arterial blood to be statistically distributed. We consider cases of (1) a uniform distribution on a finite time interval and (2) a normal distribution characterized by its mean and standard deviation. These models are physiologically meaningful because the statistical nature of the arrival times reflects the distribution of velocities and path lengths that the blood water molecules undertake from the tagging region to the imaged region. The model parameters can be estimated from the measured dependency of the perfusion signal on the tag inversion time.

Keywords: Perfusion; Arterial spin labeling; Input function; Arrival time; Mathematical model

1. Introduction

The Pulsed Arterial Spin Labeling (PASL) perfusion methods such as EPISTAR [1] (standing for Echo-Planar Imaging and Signal Targeting with Alternating Radiofrequency), FAIR [2,3] (Flow-sensitive Alternating Inversion Recovery), UNFAIR [4,5] (UN-inverted FAIR), PICORE [6] (Proximal Inversion with Control for Off-Resonance Effects), TILT [7] (Transfer Insensitive Labeling Technique), or QUIPSS II [8] (QUantitative Imaging of Perfusion using a Single Subtraction) provide a non-invasive means to assess the human cerebral blood perfusion without the need for excessive RF power or special RF coil design. They can thus be easily implemented on common clinical systems.

The PASL results are often presented in terms of a difference between the flow-weighted and control images. More quantitative assessment of the perfusion requires a mathematical model, usually originating from a modified version of the Bloch equations [9] that takes into account the incoming and outgoing spins carried by blood flow. Typically, an instant and uniform arrival of the tagged blood has been assumed [2,10]. For multi-slice imaging, the effect of a delayed arrival of the tagged spins into the imaging slice has been considered [11]. A very general model for perfusion imaging has been developed by Buxton et al. [12], who incorporated an arbitrarily shaped arterial input function. They also included analytical solutions for several simple cases. More general examples were handled numerically.

Here we present analytical solutions for two more general cases of the arterial blood input function. The wavefront of the arriving tagged blood is no longer assumed to form a sharp-edged step function. Instead, we account for the statistical nature of the arrival times, thus accommodating the physiological variability of the blood velocities and path lengths. This approach leads to smoothing of the tagged blood wavefront, the exact shape of which depends on the statistical distribution used. We consider two cases that are simple enough to be solved analytically, a uniform distribution and a normal distribution.

* Corresponding author. Fax: 1-845-398-5472.
E-mail address: hrabe@mail.magalien.com (J. Hrabe).

1090-7807/$ - see front matter © 2003 Elsevier Inc. All rights reserved.
doi:10.1016/j.jmr.2003.11.002

If the RF tagging of the arterial blood has a limited spatial extent as is usual, e.g., for common transmit/receive head coils, the arterial input function is truncated. Neglecting this effect can lead to considerable errors, especially for longer mixing times [13]. Similar dissipation and smoothing then applies to the trailing edge of the tagged blood except that the effect is larger due to larger distances and arrival times involved.

2. Theory

The PASL techniques typically acquire two images which correspond to the flow-weighted magnetization M_F (when the arterial blood is tagged by an RF pulse), and the control magnetization M_C (with no tagging). A modified Bloch equation for M_F in an imaged voxel is

$$\frac{dM_F(t)}{dt} = \frac{M_0 - M_F(t)}{T_1} + fM_{aF}(t) - \frac{f}{\lambda}M_F(t), \quad M_F(0) = 0, \tag{1}$$

where M_0 is the equilibrium magnetization, $M_{aF}(t)$ is the tagged arterial input magnetization, T_1 is the tissue spin–lattice relaxation constant, f is the perfusion flow in s^{-1}, and λ is the blood/tissue water partition coefficient [9].

A similar equation for the control magnetization M_C is

$$\frac{dM_C(t)}{dt} = \frac{M_0 - M_C(t)}{T_1} + fM_{aC}(t) - \frac{f}{\lambda}M_C(t), \quad M_C(0) = 0. \tag{2}$$

Rather than solving directly Eqs. (1) and (2), it is convenient to consider a differential equation for the difference intensity $D(t) = M_F(t) - M_C(t)$ which can be written as

$$\frac{dD(t)}{dt} + \frac{D(t)}{T_{1app}} = D_a(t), \quad D(0) = 0, \tag{3}$$

where

$$\frac{1}{T_{1app}} = \frac{1}{T_1} + \frac{f}{\lambda} \quad \text{and} \quad D_a(t) = f[M_{aF}(t) - M_{aC}(t)].$$

If spin tagging is achieved by an inversion pulse and the repetition time is sufficiently longer than the longitudinal relaxation times of blood and tissue, the right side of Eq. (3) can be expressed as

$$D_a(t) = 2M_0\frac{f}{\lambda}\exp\left(-\frac{t}{T_{1b}}\right)W(t), \tag{4}$$

where T_{1b} is the relaxation constant of blood, and $W(t)$ describes the arterial blood input function (which can also incorporate inversion pulse imperfections). The numerical factor of 2 would disappear if the tagging was achieved by a saturation pulse instead of inversion. This model can be applied to all PASL techniques mentioned in Section 1.

Various approximations, e.g., $T_{1app} \approx T_1$ or even $T_{1app} \approx T_1 \approx T_{1b}$, have been made in various PASL models, leading to a range of solutions for the $D(t)$ signal. The largest source of variability, however, stems from the arterial blood input function $W(t)$ that describes the time course of the tag proportion among all the blood arriving to the imaged voxel. It ranges from 0 to 1.

The general solution of Eq. (3) can be expressed, thanks to its simple initial condition, as a convolution of the right-hand side $D_a(t)$ with kernel $D_\delta(t)$ which satisfies Eq. (3) with Dirac delta function on the right-hand side ($D_a(t) = \delta(t)$):

$$\begin{aligned} D(t) &= D_a(t) * D_\delta(t) \\ &= \int_0^\infty D_a(t-t')\exp\left(-\frac{t'}{T_{1app}}\right)dt', \end{aligned} \tag{5}$$

where

$$D_\delta(t) = \begin{cases} 0 & \text{for } t < 0 \quad \text{and} \\ \exp\left(-\frac{t}{T_{1app}}\right) & \text{for } t \geqslant 0. \end{cases}$$

2.1. Boxcar input function

If the dissipation of the tagged region edges is neglected, the input function becomes simply

$$W(t) = \begin{cases} \alpha & \text{for } \tau_1 \leqslant t \leqslant \tau_2 \quad \text{and} \\ 0 & \text{elsewhere.} \end{cases} \tag{6}$$

The parameters τ_1 and τ_2 denote the arrival time of the leading and trailing edge of the tagged blood, respectively, and α is the inversion efficiency ($0 < \alpha < 1$). The implicit assumption is that the tagged blood moves as a rectangular block into the imaging slice.

Substitution of $W(t)$ into Eq. (4) and subsequent integration in Eq. (5) leads to the solution

$$D(t) = \begin{cases} 0 & \text{for } t < \tau_1, \\ \frac{F}{R}(\exp(Rt) - \exp(R\tau_1)) & \text{for } \tau_1 \leqslant t \leqslant \tau_2, \quad \text{and} \\ \frac{F}{R}(\exp(R\tau_2) - \exp(R\tau_1)) & \text{for } \tau_2 < t, \end{cases} \tag{7}$$

where

$$R = \frac{1}{T_{1app}} - \frac{1}{T_{1b}} \quad \text{and} \quad F = 2\alpha M_0\frac{f}{\lambda}\exp\left(-\frac{t}{T_{1app}}\right).$$

This solution is termed a "standard model" in [12] (their Eq. (3)).

2.2. Uniform dissipation of input function

The tagged blood water molecules proceed to the imaging slice along pathways of varying lengths and at different speeds. This inherent randomness has a consequence of smoothing the edges of the input function.

As the simplest possible approximation, we assume that a tag concentrated at a single point source would dissipate into a homogeneously filled sphere with radius σ. Because the leading edge of the tagged region is originally formed by a plane parallel with the imaging slice, the dissipation is equivalent to a 1D convolution of the Heaviside step function with a boxcar of width 2σ. When considering separately the leading and the trailing edges of the standard model described in the previous paragraph, the dissipative smoothing results in a trapezoid input function

$$W(t)=\begin{cases}0 & \text{for } t<\tau_1^-,\ \frac{\alpha}{2}+\frac{\alpha}{2\sigma_1}(t-\tau_1)\\ & \text{for } \tau_1^-\leqslant t<\tau_1^+,\\ \alpha & \text{for } \tau_1^+\leqslant t<\tau_2^-,\ \frac{\alpha}{2}-\frac{\alpha}{2\sigma_2}(t-\tau_2)\\ & \text{for } \tau_2^-\leqslant t<\tau_2^+,\quad \text{and}\\ 0 & \text{for } \tau_2^+\leqslant t,\end{cases} \tag{8}$$

where

$$\tau_1^-=\tau_1-\sigma_1,\quad \tau_1^+=\tau_1+\sigma_1,\quad \tau_2^-=\tau_2-\sigma_2,$$
$$\tau_2^+=\tau_2+\sigma_2.$$

The trailing edge will generally be more dissipated due to its larger distance from the imaging slice. However, we assume for the sake of simplicity that the characteristic length of the input function $(\tau_2-\tau_1)$ exceeds the duration $(\sigma_1+\sigma_2)$.

The piece-wise solution on the identical time intervals can be expressed as

$$D(t)=\begin{cases}0,\\ \frac{F}{R}\left(\frac{t-\tau_1^-}{2\sigma_1}\exp(Rt)+\frac{\exp(R\tau_1^-)-\exp(Rt)}{2R\sigma_1}\right),\\ \frac{F}{R}\left(\exp(Rt)+\frac{\exp(R\tau_1^-)-\exp(R\tau_1^+)}{2R\sigma_1}\right),\\ \frac{F}{R}\left(\exp(Rt)+\frac{\exp(R\tau_1^-)-\exp(R\tau_1^+)}{2R\sigma_1}-\frac{t-\tau_2^-}{2\sigma_2}\right.\\ \qquad\left.\times\exp(Rt)-\frac{\exp(R\tau_2^-)-\exp(Rt)}{2R\sigma_2}\right),\\ \frac{F}{R}\left(\frac{\exp(R\tau_1^-)-\exp(R\tau_1^+)}{2R\sigma_1}-\frac{\exp(R\tau_2^-)-\exp(R\tau_2^+)}{2R\sigma_2}\right).\end{cases} \tag{9}$$

In contrast to the standard model with the boxcar input function, the difference signal has a continuous derivative with respect to time. It is easy to verify that the standard model represents a limit case of Eq. (9) for $\sigma_1\to 0$ and $\sigma_2\to 0$.

2.3. Gaussian dissipation of input function

The obvious disadvantage of the uniform dissipation is the cumbersome piece-wise character of the result. The uniform point source dissipation is also unlikely in a living organism. These drawbacks can be remedied by assuming that any tag point source dissipates into a shape of a Gaussian normal distribution with standard deviation σ. The sharp wavefront edge of the input function therefore undergoes Gaussian smoothing:

$$H(t)*\frac{\exp\left(-\frac{t^2}{2\sigma^2}\right)}{\sqrt{2\pi}\sigma}=\frac{1}{2}+\frac{1}{\sqrt{\pi}}\int_0^{\frac{t}{\sqrt{2}\sigma}}\exp(-\vartheta^2)\,\mathrm{d}\vartheta$$
$$=\frac{1}{2}\left[1+\operatorname{erf}\left(\frac{t}{\sqrt{2}\sigma}\right)\right],$$

where $H(t)$ is a Heaviside step function and $\operatorname{erf}(t)$ is the error function. A sufficiently long boxcar input can be treated as an appropriate subtraction of two step functions at times τ_1 and τ_2 with independent dissipations of the leading and trailing edges characterized by standard deviations σ_1 and σ_2, respectively. We thus obtain an input function

$$W(t)=\frac{\alpha}{2}\left[\operatorname{erf}\left(\frac{t-\tau_1}{\sqrt{2}\sigma_1}\right)-\operatorname{erf}\left(\frac{t-\tau_2}{\sqrt{2}\sigma_2}\right)\right]. \tag{10}$$

The leading wavefront of the tagged region arrives with an average delay τ_1, while an average delay of the trailing wavefront is τ_2.

After substituting $D_a(t)$ from Eq. (4), the input function $W(t)$ above can be integrated analytically (see, e.g., Eq. (7.4.36) on p. 304 in [14]) in Eq. (5) to obtain the time course of the perfusion signal

$$D(t)=\frac{F}{2R}\left\{[\operatorname{erf}(u_1)-\operatorname{erf}(u_2)]\exp(Rt)\right.$$
$$-\left[1+\operatorname{erf}\left(u_1-\frac{R\sigma_1}{\sqrt{2}}\right)\right]\exp\left(R\left(\tau_1+\frac{R\sigma_1^2}{2}\right)\right)$$
$$\left.+\left[1+\operatorname{erf}\left(u_2-\frac{R\sigma_2}{\sqrt{2}}\right)\right]\exp\left(R\left(\tau_2+\frac{R\sigma_2^2}{2}\right)\right)\right\}. \tag{11}$$

Here we used abbreviations

$$u_1=\frac{t-\tau_1}{\sqrt{2}\sigma_1},\quad \text{and}\quad u_2=\frac{t-\tau_2}{\sqrt{2}\sigma_2}.$$

The difference signal and its time derivative are continuous functions of time. The standard model of Eq. (7) can again be obtained as a special limit case ($\sigma_1\to 0$ and $\sigma_2\to 0$) of Eq. (11).

3. Results

To demonstrate the influence of model parameters on the predicted subtraction signal, we calculated $D(t)$ using Eq. (9) (Fig. 1) and Eq. (11) (Fig. 2) for the uniform and Gaussian dissipation, respectively. The parameters were chosen to approximate PASL perfusion imaging at 1.5 T ($T_1=0.9$ s, $T_{1b}=1.2$ s, $\lambda=0.9$, $f=0.015\,\mathrm{s}^{-1}$, and $\alpha=0.9$). Fully relaxed magnetization was set to $M_0=100$ to obtain the difference signal as a percentage of M_0. We assumed that σ is proportional to the square root of time, analogously to a diffusion. Dissipation width σ_2 was therefore always set to $\sigma_1\sqrt{\tau_2/\tau_1}$ to

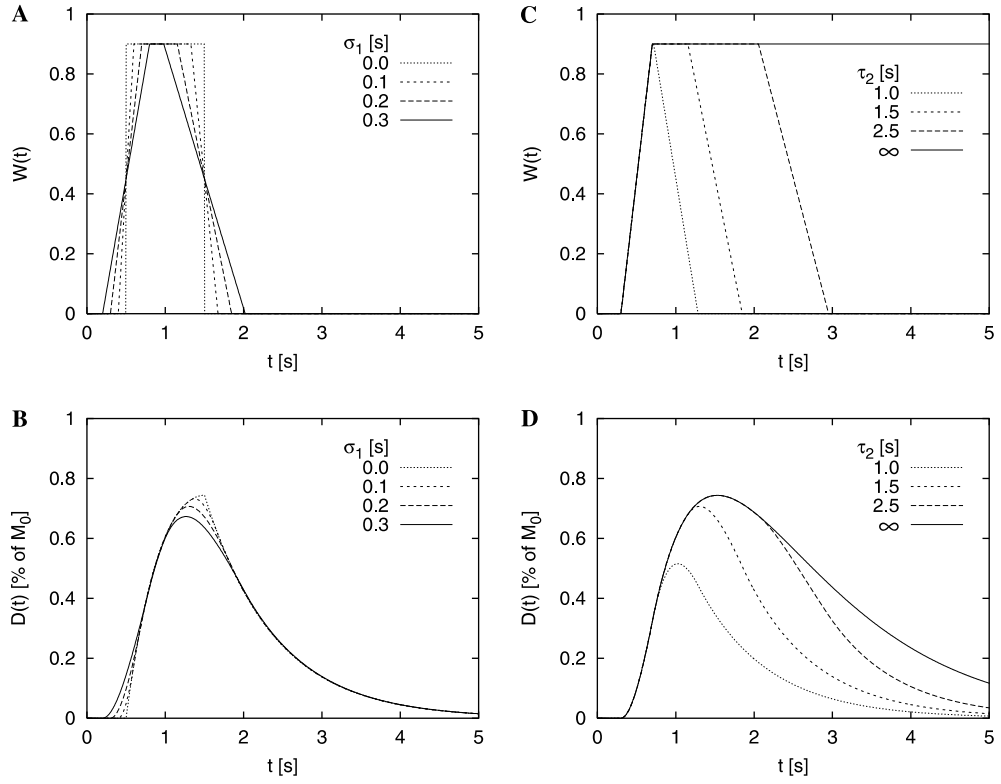

Fig. 1. Uniform dissipation model. (A) Examples of trapezoid input functions with σ_1 from 0 (equivalent to a boxcar input) to 0.3 s; $\tau_1 = 0.5$ s and $\tau_2 = 1.5$ s. The trailing wavefront dissipation was set to $\sigma_2 = \sigma_1\sqrt{\tau_2/\tau_1}$. (B) Perfusion signal corresponding to the input functions in A. (C) Trapezoid input functions with varying extent of the tagged region ($\sigma_1 = 0.2$ s, τ_2 from 1 s to ∞). (D) The corresponding perfusion signal curves.

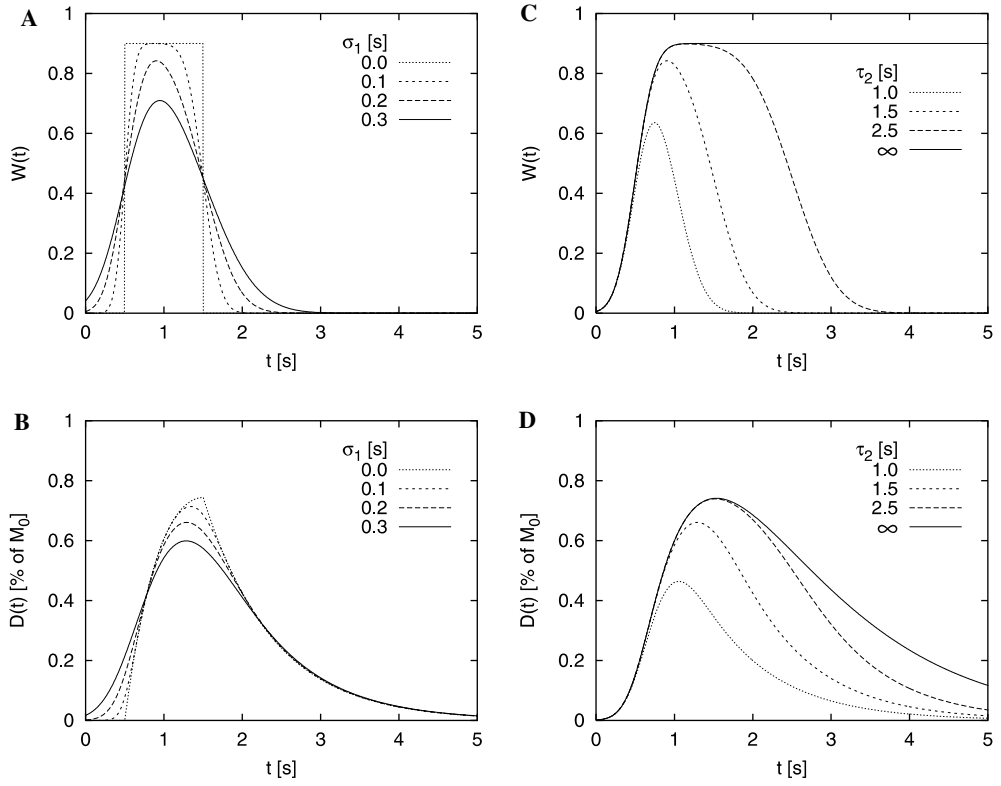

Fig. 2. Gaussian dissipation model. All the parameters used to construct curves in (A–D) are identical to those used in the corresponding panels of Fig. 1.

account for larger spread of the trailing edge. A notable exception was the QUIPSS II model, where $\sigma_1 = \sigma_2$.

Fig. 1 summarizes the results of simulations with the trapezoid input function. The left column (A and B) shows the influence of changing dissipation width σ_1. The mean tag arrival (τ_1) and departure (τ_2) times are typical for PASL imaging with a standard head coil. However, it is clear that any differences at longer times are eventually lost in T_1 relaxation process of the tag. Compared to a boxcar input function with the same arrival and departure times, the signal is initially rising with lower slope and reaches a lower maximum value.

The right column of Fig. 1 (C and D) shows the dramatic effect of varying the tagged region extent. For a very narrow region, the maximum perfusion signal is shifted to an earlier time and it is much lower than the optimum signal which would be obtained with wide tagged region (e.g., with a body coil). Unlike for the boxcar input function, the difference signal time course is smooth everywhere, a result of a continuous derivative.

Analogous simulations with Gaussian dissipation are depicted in the four panels of Fig. 2. The input functions are smoother than their trapezoidal counterparts and for higher values of σ_1, the curves never reach the plateau of $W(t) = \alpha$ before they fall again. The effect of Gaussian input smoothing on the perfusion signal is similar to the uniform smoothing but it is larger, clearly affecting both the initial slope and the maximum value. The effect on maximum difference signal is as large as 20% compared to the boxcar input, for a modest dissipation value of $\sigma_1 = 200$ ms.

The effect of the tagged region width is characterized in Figs. 2C and D. The behavior is very similar to that shown in Figs. 1C and D but the perfusion curves are wider.

All three models with no dissipation, uniform dissipation, and Gaussian dissipation are directly compared in Fig. 3. The input functions (A) have identical time characteristics in terms of their mean arrival and departure times and the last two models also in terms of σ_1 and σ_2. Yet the perfusion signals (B) differ significantly among them for almost the entire first 2 s. Any differences then succumb to a longitudinal relaxation process. Gaussian dissipation leads to the lowest maximum signal reached along the lowest initial slope.

The QUIPSS II method [8] was developed to eliminate dependency of the perfusion signal on the arrival time τ_1. The tag region is saturated at a fixed time $\delta\tau$ after the initial inversion. It is assumed that the inversion and saturation pulses have identical profiles and that the saturation is applied before any fresh blood could traverse the tagged region and escape saturation. In this case, the $W(t)$ function becomes better defined than in other PASL methods—it is now symmetrical ($\sigma_1 = \sigma_2 = \sigma$), and the difference between the mean arrival times $\tau_2 - \tau_1 = \delta\tau$ is known and fixed. Fig. 4 shows

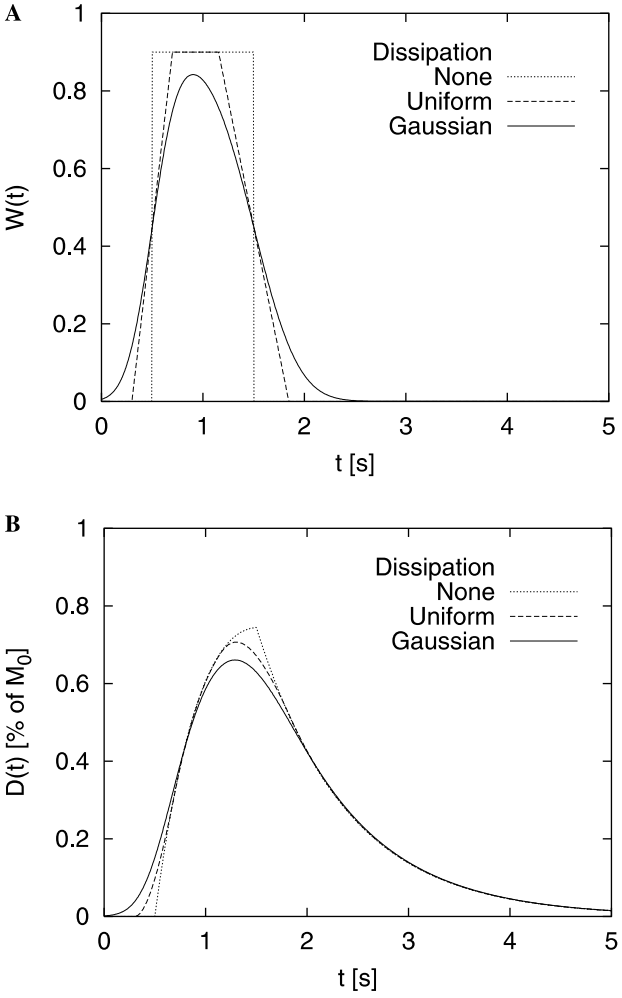

Fig. 3. A direct comparison of the three models with no dissipation, uniform dissipation, and Gaussian dissipation. The parameters were chosen to resemble PASL perfusion measurement with a standard transmit/receive head coil at 1.5 T ($T_1 = 0.9$ s, $T_{1b} = 1.2$ s, $\lambda = 0.9$, $f = 0.015\,\mathrm{s}^{-1}$, $\alpha = 0.9$, $\tau_1 = 0.5$ s, $\tau_2 = 1.5$ s, $\sigma_1 = 0.2$ s, and $\sigma_2 = 0.35$ s). Perfusion signal curves in B result from input functions in A.

several time courses of the QUIPSS II perfusion signal for different arrival times and $\delta\tau = 0.6$ s. If the images are taken at time $t > \tau_{1\max} + \delta\tau + \sigma_{\max}$, the dependency on τ_1 and σ_1 becomes negligible (and would disappear completely if $T_{1app} = T_1 = T_{1b}$). This advantage is traded for perfusion signal loss. Randomization of arrival times makes the QUIPSS II assumptions harder to satisfy. The saturation pulse may have to be applied earlier due to dissipation of the distal edge of the tagged region, and the acquisition has to be further delayed by the maximum σ found in the image.

4. Discussion and conclusions

We have theoretically investigated the effect of arrival time randomization on the perfusion signal in the PASL

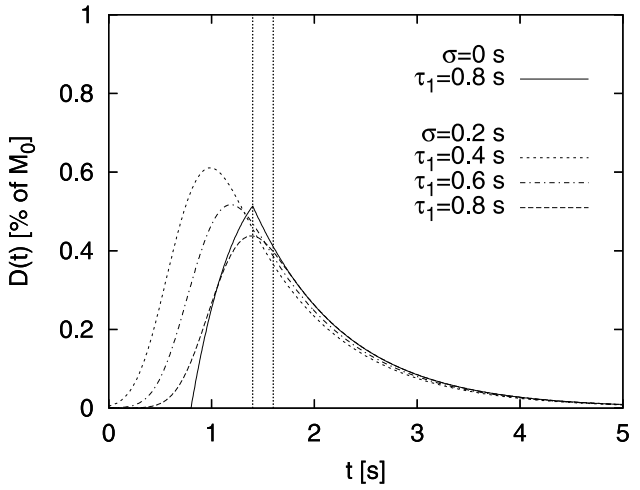

Fig. 4. Gaussian dissipation model for a typical QUIPSS II acquisition. Maximum τ_2 is $\tau_{1\,\max} + \delta\tau = 0.8 + 0.6$ s. Other parameters are the same as specified in Fig. 3. The vertical dotted lines mark the minimum recommended acquisition time for standard model ($\sigma = 0$ s, left line) and Gaussian dissipation model ($\sigma = 0.2$ s, right line). The remaining differences in the perfusion signal at later times are due to mutually unequal relaxation times $T_{1\mathrm{app}}$, T_1, and $T_{1\mathrm{b}}$.

techniques. It was previously reported [12] that input functions with smoother edge shape than a boxcar may affect the initial slope of the perfusion signal. We have demonstrated how this input function smoothing may occur and that it can affect not only the initial slope but also the maximum obtainable perfusion signal. The effect of randomization is particularly large when the tagged region is narrow (approximating, e.g., the use of a standard head coil for tag excitation). Employing the boxcar model in this situation would underestimate the perfusion.

The model treats the leading and trailing wavefronts of the tagged blood separately, with their own respective time shifts and dissipations. An analogy with the diffusion process suggests that if the dissipation is sufficiently homogeneous in the combined volume of the tagging and imaging regions, the standard deviations σ_1 and σ_2 should satisfy the relationship

$$\frac{\sigma_2}{\sigma_1} = \sqrt{\frac{\tau_2}{\tau_1}}.$$

We used this relationship in all of our simulations, except for the QUIPSS II model.

Both the uniform and Gaussian dissipations lead to qualitatively similar effects in the perfusion signal. Our first choice, however, is the Gaussian model. There is a large number of random effects on the arrival times [15]. In larger vessels, viscosity, pulsation and turbulence lead to dispersion of velocities. As the tagged blood reaches smaller vessels, total cross-sectional area increases and the flow slows down (e.g., by a factor of 100). Countless bifurcations lend the blood supply tree a fractal character [16]. Velocity magnitude variations are smaller but directions become highly randomized. An imaging voxel is typically large (e.g., 125 mm^3) and is therefore reached by many different pathways. Although there is currently no widely accepted statistical description of this complex process with respect to tag arrival times, a convection-dispersion equation with a diffusion-like dissipation term has been applied to the blood circulation problem and experimentally validated [17]. The Gaussian dissipation therefore likely represents a reasonable first approximation until more definitive experimental evidence is established.

While we have discussed only PASL perfusion, it is clear that similar dissipation of arrival times influences the Continuous Arterial Spin Labeling (CASL) methods as well. Consider the steady state situation after long continuous inversion tagging. Eq. (3) will lose the time derivative and its right-hand side $D_{\mathrm{a}}(t \to \infty)$ will have to be obtained by averaging over all possible arrival times. For Gaussian distribution with mean arrival time τ and standard deviation σ we get

$$\begin{aligned} D(t \to \infty) &= T_{1\mathrm{app}} D_{\mathrm{a}}(t \to \infty) \\ &= T_{1\mathrm{app}} 2\alpha M_0 \frac{f}{\lambda} \frac{1}{\sqrt{2\pi}\sigma} \int_{-\infty}^{\infty} \exp\left(-\frac{t'}{T_{1\mathrm{b}}} - \frac{(t'-\tau)^2}{2\sigma^2} \right) \mathrm{d}t' \\ &= T_{1\mathrm{app}} 2\alpha M_0 \frac{f}{\lambda} \exp\left(-\frac{\tau}{T_{1\mathrm{b}}} \right) \exp\left(\frac{\sigma^2}{2T_{1\mathrm{b}}^2} \right). \end{aligned} \tag{12}$$

This solution differs from the standard CASL model with uniform arrival time (Eq. (5) in [12]) by a factor of $\exp(\sigma^2/(2T_{1\mathrm{b}}^2)) > 1$. The perfusion flow is therefore overestimated whenever the dissipation of arrival times is present. E.g., for $T_{1\mathrm{b}} = 1.2$ s and $\sigma = 0.3, 0.6$, and 0.9 s this factor is 1.03, 1.13, and 1.32, respectively. For large distances between the tagging plane and the image plane, the randomization of the arrival times can thus become a significant factor for the CASL methods as well.

The perfusion model proposed here is an improvement of the standard boxcar model which takes into account some effects that have been neglected so far. These include the statistical distribution of the arterial blood arrival times, imperfect edges of the tagging RF profiles, and the effect of limited spatial extent of the transmit coil. Ignoring these effects can in some cases lead to inaccurate perfusion estimates. The analytical solutions provided here make it easy to estimate their influence under various circumstances.

References

[1] R.R. Edelman, B. Siewert, D.G. Darby, V. Thangaraj, A.C. Nobre, M.M. Mesulam, S. Warach, Qualitative mapping of cerebral blood flow and functional localization with echo-planar MR imaging and signal targeting with alternating radio frequency, Radiology 192 (2) (1994) 513–520.

[2] K.K. Kwong, D.A. Chesler, R.M. Weisskoff, K.M. Donahue, T.L. Davis, L. Ostergaard, T.A. Campbell, B.R. Rosen, MR

perfusion studies with T1-weighted echo planar imaging, Magn. Reson. Med. 34 (6) (1995) 878–887.
[3] S.G. Kim, Quantification of relative cerebral blood flow change by flow-sensitive alternating inversion recovery (FAIR) technique: application to functional mapping, Magn. Reson. Med. 34 (3) (1995) 293–301.
[4] J.A. Helpern, C.A. Branch, M.N. Yongbi, N.C. Huang, Perfusion imaging by un-inverted flow-sensitive alternating inversion recovery (UNFAIR), Magn. Reson. Imaging 15 (2) (1997) 135–139.
[5] S.S. Berr, V.M. Mai, Extraslice spin tagging (EST) magnetic resonance imaging for the determination of perfusion, J. Magn. Reson. Imaging 9 (1) (1999) 146–150.
[6] E.C. Wong, R.B. Buxton, L.R. Frank, Implementation of quantitative perfusion imaging techniques for functional brain mapping using pulsed arterial spin labeling, NMR Biomed. 10 (4-5) (1997) 237–249.
[7] X. Golay, M. Stuber, K.P. Pruessmann, D. Meier, P. Boesiger, Transfer insensitive labeling technique (TILT): application to multislice functional perfusion imaging, J. Magn. Reson. Imaging 9 (3) (1999) 454–461.
[8] E.C. Wong, R.B. Buxton, L.R. Frank, Quantitative imaging of perfusion using a single subtraction (QUIPSS and QUIPSS II), Magn. Reson. Med. 39 (5) (1998) 702–708.
[9] D.S. Williams, J.A. Detre, J.S. Leigh, A.P. Koretsky, Magnetic resonance imaging of perfusion using spin inversion of arterial water, Proc. Natl. Acad. Sci. USA 89 (1) (1992) 212–216.
[10] J.L. Tanabe, M. Yongbi, C. Branch, J. Hrabe, G. Johnson, J.A. Helpern, MR perfusion imaging in human brain using the UNFAIR technique, J. Magn. Reson. Imaging 9 (6) (1999) 761–767.
[11] Y. Yang, J.A. Frank, L. Hou, F.Q. Ye, A.C. McLaughlin, J.H. Duyn, Multislice imaging of quantitative cerebral perfusion with pulsed arterial spin labeling, Magn. Reson. Med. 39 (5) (1998) 825–832.
[12] R.B. Buxton, L.R. Frank, E.C. Wong, B. Siewert, S. Warach, R.R. Edelman, A general kinetic model for quantitative perfusion imaging with arterial spin labeling, Magn. Reson. Med. 40 (3) (1998) 383–396.
[13] M.L. Lipton, C.A. Branch, J. Hrabe, D.P. Lewis, J.A. Helpern, RF excitation profiles with FAIR: impact of truncation of the arterial input function on quantitative perfusion, J. Magn. Reson. Imaging 13 (2) (2001) 207–214.
[14] M. Abramowitz, I.A. Stegun, Handbook of Mathematical Functions, ninth ed., Dover Publications, New York, 1972.
[15] D.A. McDonald, Blood Flow in Arteries, second ed., Williams and Wilkins, Baltimore, 1974.
[16] G.B. West, J.H. Brown, B.J. Enquist, A general model for the origin of allometric scaling laws in biology, Science 276 (5309) (1997) 122–126.
[17] A. Dokoumetzidis, P. Macheras, A model for transport and dispersion in the circulatory system based on the vascular fractal tree, Ann. Biomed. Eng. 31 (3) (2003) 284–293.